Surface Studies of Ceria and Mesoporous Ceria Powders by Solid-State ^{1}H MAS NMR

Daniel M. Lyons, James P. McGrath, and Michael A. Morris*

Department of Chemistry, University College Cork, Cork, Republic of Ireland

Received: January 21, 2003; In Final Form: March 26, 2003

Herein is described the first detailed study of ceria surfaces using ^{1}H MAS NMR techniques to probe the nature of hydroxyl species formed after exposure to water. The ^{1}H MAS NMR signal deriving from adsorbed hydroxyl species was used to probe the surface of ceria and crystalline mesoporous powders as a function of calcination temperature. It was found that the signals from all samples were well-resolved and of high intensity and showed easily observed chemical shifts depending on their environment. High surface areas were evidenced by large hydroxyl-derived ^{1}H peak integrals for the mesoporous samples compared to that of ceria prepared by traditional precipitation techniques. It is suggested that surface-adsorbed hydroxyl species generally occupy two distinct structural environments (on-top and bridge) on ceria surfaces. Hydroxyl groups assigned to on-top positions were found to be more mobile and desorbed at lower temperatures than those held in bridging positions. In addition, the mesoporous surface appears to comprise of two distinct regions assigned to external surfaces and internal pore and cavity surfaces. We also highlight a more general point that adsorbate probe MAS NMR techniques can provide important analysis of surface chemistry in favorable circumstances. Ceria is an ideal example in which very well-resolved intense ^{1}H signals from adsorbed hydroxyl species are observed, and consequently MAS NMR methods provide unique details of the surface chemistry. The relevance of these data is discussed in the context of current knowledge of the properties of ceria.

Introduction

Cerium (in both the Ce^{3+} and Ce^{4+} oxidation state and as the oxidative couple between these species) is finding increasing use in important technological systems such as superconductors[1] and as an important component in catalytic systems[2,3] and is thought will be one of the materials of choice as the solid electrolyte in future solid oxide fuel cells.[4] Cerium-containing materials are also being used to probe fundamental materials properties such as magnetic−electronic interactions.[5] Previous investigations on the macroscopic scale have focused on cerium dioxide's (ceria, CeO_2) remarkable redox chemistry and oxygen storage capacity, but only relatively recently have significant studies been carried out on the nano- and quantum scales.[6] It is thought that the ability either to prepare nanocrystalline particles or to manipulate the architecture of ceria on the nanometer scale will generate materials with novel properties including enhanced electronic, ionic, and catalytic abilities.[7] There is now considerable interest in preparing thin films of ceria because of their optoelectronic properties.[8] In the area of catalysis, nanocrystalline ceria (by virtue of its high surface area) is considered a potential candidate for forming novel catalytic materials as it allows for both increased dispersion of active secondary components such as noble metals and provides for unusual defect chemistry.[9]

Recently, we have reported the preparation of high surface area mesoporous ceria and structural studies showed that the walls of this material were essentially crystalline with a high degree of long-range order.[10] In common with most authors the study was based on physical characterization of the architecture. It is more difficult to study the surface chemistry, particularly the electronic environment, as these materials are not suited to some common surface analysis techniques since they are powders, and the preparation of highly defined surfaces is essentially impossible. These nanocrystalline mesoporous materials comprise of hindered or strained surface regions due to pores and semienclosed cavities where electronic effects may be significantly different from those on ideal crystal planes. Indeed, it is the surface structure and electronic properties at ceria−metal interfaces that are thought to be one of the keys to the functioning of multicomponent catalytic systems such as, for example, Rh/CeO_2.[11,12] Therefore, there is a need to describe the electronic environment of such materials to contribute to a greater understanding of the unique chemistry of ceria. Solid-state MAS NMR has become an important tool for investigating the local electronic environments in many physical, chemical, and biological systems.[13−15] Perhaps the greatest advantage that solid-state NMR has offered in investigations of porous materials is that in favorable circumstances even very similar chemical species can be differentiated (by observation of resonance lines with different chemical shifts), and the observed chemical shift is sensitive to both the electronic and structural environment. Indeed, ceria seems particularly suited to MAS NMR studies because the adsorbed hydroxyl species give rise to some of the sharpest resonances seen in adsorption studies of powder surfaces. In comparison to techniques such as powder X-ray diffraction (PXRD) and transmission electron microscopy (TEM), the MAS NMR technique has been shown to be sensitive to subtle changes in structure and electronic environment. Previous MAS NMR investigations of porous materials (mainly zeolites because of the distinct structure) have focused on studies of lattice species such as ^{29}Si, ^{27}Al, and ^{31}P and provided good bulk characterization.[16] Early pioneers such as Karger et al.[17] have extended solid-state NMR to the study of porous materials by using adsorbed organic species as a surface probe in self-diffusion measurements. For example, ^{129}Xe NMR

* To whom correspondence should be addressed: Tel +353 21 4902180; Fax +353 21 4274097; e-mail m.morris@ucc.ie.

10.1021/jp0341570 CCC: $25.00
Published on Web 04/17/2003

studies using pulsed field gradient techniques have used deformation of the electron density about the nucleus as the probe for investigating mass transport in zeolite materials.[18] While this method has proven successful for investigating microporous materials, it has more recently being used as an effective probe for the pore architecture of mesoporous materials.[19] Water has also been used as a probe molecule for both microporous and mesoporous materials. Proton NMR adsorption studies of zeolite ZSM-5 have indicated proton exchange between water hydrogen-bonded to surface-bound bridging hydroxyl groups and hydroxonium species[20] while ^{1}H NMR studies of water freezing in pores[21] of mesoporous silica have shown an NMR signal dependence on the freezing temperature and hence the pore diameter. The authors of the latter work suggested a linear dependence of spin−lattice relaxation rate on the inverse pore radius. This appears to have provided a useful means for determining pore diameters of highly ordered silica mesophases. The technique is less applicable to less well ordered porous materials containing a wide distribution of pore sizes which display very broad proton resonances that cannot easily be correlated with actual pore structure. Hansen et al.[22] have alternatively proposed that the spin−lattice relaxation, and consequently the proton resonance, was dependent not only on mesopore radius but also on the number of silanol protons present, thus questioning the use of ^{1}H NMR as an accurate means for determining pore radii. Therefore, there is some controversy at present surrounding the use of NMR for determining the physical parameters of mesoporous materials, and it is clear that more work is required before a better understanding of the local structure of these materials may be gained. The work reported herein describes hydroxyl-derived ^{1}H MAS NMR studies of mesoporous ceria. There have been relatively few NMR investigations into mesoporous materials using hydroxyl-derived proton resonances as a probe for surface or pore architecture and electronic environment and to the best of our knowledge no such NMR studies of mesoporous ceria. Adsorbed hydroxy species allowed simple one-pulse NMR experiments in initial investigations of the electronic environment of surface regions of mesoporous ceria materials. This technique also allowed quantification of signal intensities. Crafting of novel ceria-based materials through more detailed understanding of its enhanced electronic or catalytic properties should allow the exploitation of such functionality that will drive the application of next-generation ceria-based materials.

Experimental Section

Mesoporous ceria samples were prepared by a surfactant-assisted approach and calcined in air at various temperatures as described previously.[10] Briefly, hexadecylamine (6 g, 0.025 mol) was used as a neutral surfactant template about which cross-linking and condensation of a cerium acetate precursor in aqueous ethylenediamine solution (50%, 35 mL) progressed. A cerium:surfactant ratio of 2 was used. Densification of this inorganic framework about the surfactant under carefully controlled hydrothermal conditions and subsequent removal of the organic template by direct calcination in air for 4 h at temperatures greater than 300 °C gave a mesoporous ceria material with surface areas of 245 $m^2\ g^{-1}$. A sample consisting of densified ceria was made by evaporation of a cerium nitrate solution (3 M). The solution was evaporated to dryness at 60 °C and the solid ground before calcination at 350 °C for 8 h. The sample was then calcined at 600 °C for a further 8 h and ground to a fine powder again. The surface area of the sample was measured at 9.7 $m^2\ g^{-1}$. This low figure suggests that porosity was small. The final calcination temperature of 600 °C was chosen because it gave low surface area, well-defined PXRD diffractograms and dense samples with a reasonably large −OH-derived ^{1}H MAS NMR signal. At higher temperatures the signal-to-noise of the spectra was poor due to low surface area and consequently smaller peaks. This sample is identified as Evap600.

For the mesoporous material, Fourier transform infrared spectroscopy (FTIR) suggested no organic species were present after calcination although the surface was covered by adventitiously adsorbed hydroxyl and carbonate species derived from ambient storage of the samples. No FTIR evidence of superoxide or peroxide formation on the ceria surface, with characteristic vibrational frequencies of 1126 and 883 cm^{-1}, respectively, was found.[23,24] Magic angle spinning proton nuclear magnetic resonance (^{1}H MAS NMR) was used to probe surface adsorbed hydroxy species as a function of calcination temperature. Radio-frequency pulses corresponding to a flip angle of 90°, a pulse width of 4.25 μs, and a pulse delay of 1 s were employed in simple single-pulse experiments, and signal saturation was never observed. This pulse delay of 1 s was found to be about 1000 times greater than the spin−lattice relaxation times. The 90° pulse angle is thus the optimum Ernst angle for data collection. Samples were placed in a 6 mm defect-free zirconia ceramic rotor with Teflon end-caps (through which had been drilled a 0.75 mm hole to allow equilibration with the flowing gas) and a PVC spinner to ensure no background ^{1}H signals were obtained. Tetramethylsilane (TMS) was used for chemical shift calibration, and the single sharp proton peak of TMS was referenced to 0 ppm. Data were collected on a Chemagnetics 300 MHz CMX-Lite instrument with rotor spin rates of 2.5−7.5 kHz used. Gas could be passed into the sample cavity via a heater stack. Prior to data collection, each sample was heated in-situ (in the NMR probe) in clean, flowing dry air to 200 °C to degas the sample of adsorbed carbonates and water. Hydroxylation of the surface was effected by cooling (to room temperature) the sample in flowing CO_2-free dry air that was saturated by passing through deionized water. A total exposure of 15 min was used. Each sample was subsequently analyzed by MAS NMR and then heated in-situ to temperatures of 50, 80, 110, 140, 160, 180, and 200 °C. The sample was allowed to equilibrate for 10 min at the required temperature before data were collected. Peak areas are measured with reference to a known amount of hexamethylbenzene, and the peak area was referenced at the start and end of each sample analysis.

Results

Densified Nonporous Ceria. The densified material Evap600 gave essentially simple ^{1}H MAS NMR signals. Typical data are shown in Figure 1 (inset shows data collected at a probe temperature of 175 °C). The spectrum is dominated by a feature at −1.2 ppm. This is derived from a hydroxyl species exhibiting a large upfield shift resulting from the adjacent cerium cation. This feature is assigned to hydroxyl species formed from hydrogen atoms at on-top positions. A further discussion of these data is made below. Small features about 23 and −23 ppm are identified as weak spinning sidebands and are equivalent to the approximately 5 kHz spinning speeds used. The low intensity of the sideband features is consistent with very high symmetry of the surface. Weak shoulders to the dominant resonance can be observed at −3.4, −0.6, and 0.5 ppm. The peak at −3.4 ppm strongly depends on the sample treatment. The longer the samples are held at probe temperature in the instrument the better resolved and intense this feature becomes. This can be

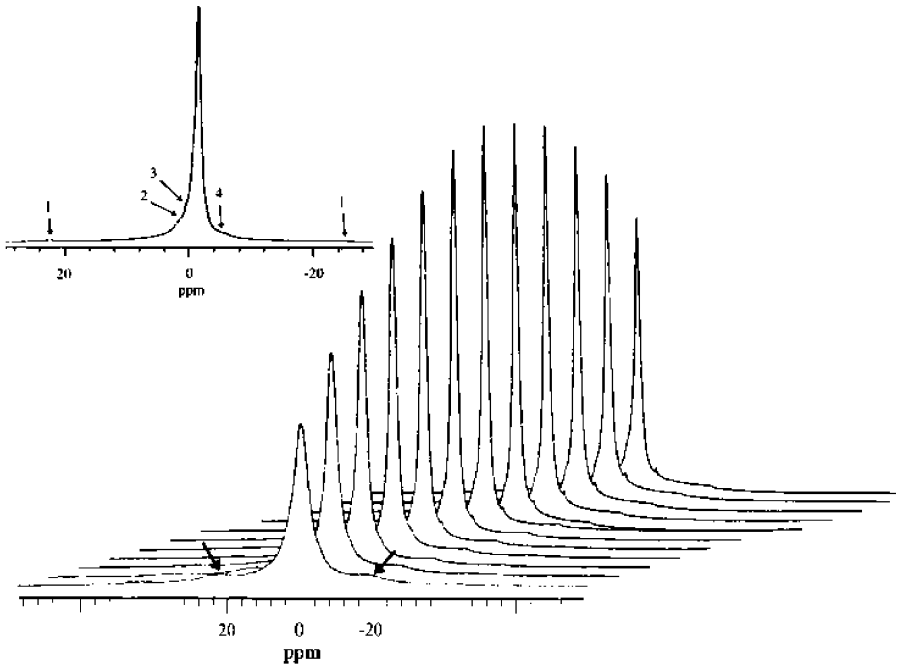

Figure 1. ^{1}H MAS NMR spectra of Evap600 sample as a function of probe temperature. The temperature increases from 0 to 220 °C (from front to back) in intervals of 20 °C. Data from a similar sample at a probe temperature of 175 °C are shown in the inset. Arrows indicate the positions of additional peaks and shoulders; 1 shows the position of weak spinning sidebands, features 2 and 3 are assigned to hydroxyls at pore surfaces, and 4 is a feature due to adsorption at point defects.

seen quite clearly in the main part of Figure 1 (stacked data as a function of probe temperature) where the extended time at probe temperature ensures it is a sharp feature. It is always a weak feature and never greater than 1/1000 of the main peak area. Work in progress in these laboratories shows that the intensity of this feature can be greatly increased by exposure to hydrogen. We suggest that this resonance of low relative intensity arises from hydroxyl features adjacent to anion vacancy sites formed by a small amount of thermal reduction/non-stoichiometry of the sample. The presence of oxygen vacancies increases the shielding of the hydrogen (and so result in the observed upfield shift of the resonance) because of the presence of the additional polaronic electrons in the surface plane. The shoulders observed at −0.6 and 0.5 ppm in the ^{1}H spectra observed for this sample are of minor intensity. Similar peaks are seen at much greater intensities from the mesoporous samples, and these are discussed below.

Figure 1 shows a stacked plot of ^{1}H spectra collected as a function of probe temperature between 25 and 225 °C. The decrease in width of signals with increasing temperature is immediately obvious. Indeed at the highest probe temperatures the measured half-width of 0.82 ppm approaches the optimal resolution (0.7 ppm) of the apparatus in this arrangement. (Techniques such as CRAMPS provided greater resolution but were not used because as they were nonquantitative.) In solid-state NMR the width of peaks largely derives from anisotropic fields and molecular motion that is slow compared to pulse times. Thus, it appears that electronic interactions between the hydrogen atoms and the lattice are very rapid although not so high as to contribute to significant lifetime broadening of the signals. T_1 spin−lattice relaxation times were measured using a simple 180° pulse, followed by 90° pulse, inversion−recovery experiment. T_1 times were measured, and the data are shown in Table 1.

For all features except for the one at −3.4 ppm, these T_1 times are rapid. Since spin−lattice relaxation arises from field fluctuations due to molecular motion, it is clear that these probed hydrogen atoms (or hydroxyl species) are mobile at the surface. It is believed that the slow relaxation time observed for the −3.4 ppm peak is consistent with the assignment made above. We suggest the much larger T_1 rates do not arise from hindered molecular motion (e.g., by adsorption at a point defect) since the peak is still very narrow and well-resolved but rather from electronic effects. These interactions are weak for Ce^{4+} ions as CeO_2 is in a closed shell configuration. However, if an anion vacancy is formed, this is accompanied by the creation of two polaronic electrons—these are long-lived states associated with Ce^{4+} cations adjacent to the vacancy, forming effectively Ce^{3+} states.[13] These data suggest that the lifetime (before a "hop" to another cerium cation) is of the order of 4 s.

TABLE 1: Spin−Lattice (T_1) Times for ^{1}H Hydroxyl-Derived MAS NMR Signals on Nonporous Low Surface Area Ceria Powder

peak position (ppm)	0.5	0.6	1.2	3.4
T_1 time (s)	2.9×10^{-3}	2.7×10^{-3}	0.8×10^{-3}	3.7×10^{-3}

The degree of motion in this system can be measured from the data presented in Figure 1. Simply by plotting the logarithm of half-width of the ^{1}H signal (from the on-top hydroxyl species) as a function of reciprocal probe temperature, a simple Arrhenius plot with a slope of 23.8 kJ mol^{-1} is obtained. This value is very close to the value of 21 kJ mol^{-1} obtained for bulk migration of oxygen species in ceria via anion vacancy movement. Thus, the results presented here are consistent with the species under investigation being −OH moieties which rapidly diffuse across the surface at room temperature. There is no evidence these species are loosely held water molecules as one would expect the activation energies to be of the same order of magnitude as in self-diffusion of water.[25] For comparative purposes, these activation energies of about 1.2 kJ mol^{-1} have been measured.

Mesoporous Ceria. Mesoporous ceria samples prepared by the neutral supramolecular templating route outlined above using

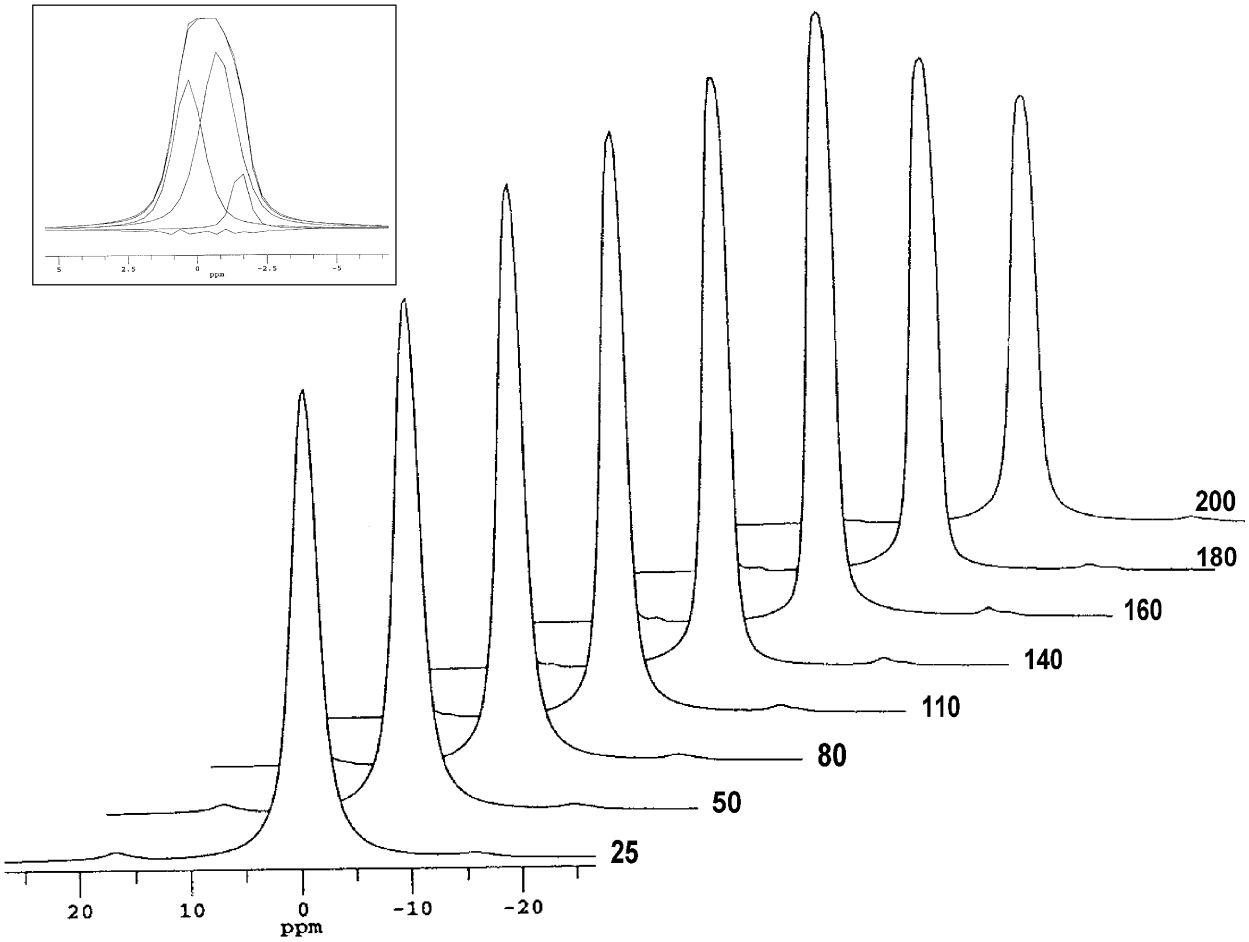

Figure 2. ^{1}H MAS NMR data collected at a series of in-situ temperatures (in °C) for mesoporous ceria after calcination at 300 °C. Inset shows the curve-fitted ^{1}H MAS NMR resonance for surface-adsorbed hydroxyl species at 180 °C with the residual plot as the "noisy" baseline under the peak envelope.

cerium acetate and hexadecylamine precursors were calcined in air (external to the NMR instrument) at temperatures of 300, 400, 500, and 600 °C for 4 h, and a series of ^{1}H MAS NMR data were obtained for each sample. These samples are referenced in the text below as Neut300, Neut400, Neut500, and Neut600, respectively.

It was found, and discussed previously, that these mesoporous ceria materials prepared from cerium acetate and hexadecylamine precursors exhibit well-defined arrays of pores with hexagonal ordering prior to surfactant removal.[10] PXRD data suggested that the walls of the material were essentially single-crystal sheets of ceria with the surface plane orientated in the <111> direction. Some pore collapse was observed after surfactant removal due to strain within the structure although a degree of mesoporosity was retained at temperatures of up to 600 °C. The optimal degree of mesoporosity was found at calcination temperatures around 400 °C. It is thought that the use of an acetate precursor favored the formation of a mesoporous framework due to the abilities of acetate chains to direct the interaction with template micelles in solution. Mesoporous ceria prepared from other ceria salts such as cerium chloride, or other surfactants such as hexadecyltrimethylammonium bromide, did not yield such a stable ordered mesoporous array, and significant collapse was observed after template removal.[26] This may have partly been due to the poor framework directing abilities of the chloride salt and the lack of formation of a densified and cross-linked inorganic matrix.

For the sample Neut300, scans were collected at various "in-situ" temperatures, and the ^{1}H MAS NMR spectra recorded are shown in Figure 2. Qualitatively, the data are similar to those shown in Figure 1. Typically, one intense peak was obtained but now appeared at a chemical shift of −0.3 ppm. However, while the peak width at room temperature (full width at half-maximum, fwhm = 2.3 ppm) is around that observed for the nonporous sample, there is only limited narrowing with increasing probe temperature (at 140 °C fwhm = 3.0 ppm). On careful inspection (see Figure 2, inset) it can be seen that the peak shape cannot be described as simple Gaussian, Lorenzian, or mixtures thereof and is asymmetrical. Apart from minor peak contributions, the peaks shown in Figure 1 are symmetrical and closely fitted by simple Gaussian peaks.

Since T_1 values of about 10^{-3} s are recorded for this feature suggesting high mobility, we believe that the peak is made up from a number of distinct contributions. Individual contributions were found by careful peak-fitting. Experimentally determined peak envelopes were "best-fitted" using software-generated peaks whose peak height, peak position, width and % Gaussian or Lorenzian (this was fixed at a 70:30 ratio that was found optimal for data in Figure 1) peak shape so that the difference between obtained peak and simulated peak was "minimized" as indicated by a sum of residuals. Within this fitting framework great care was taken to make the analysis meaningful. It might be expected that for an individual feature, e.g., on-top hydroxyls at a well-ordered exterior surface (i.e., not a pore surface), its exact width and position will be dependent on the surface

TABLE 2: Measured Peak Integrals (Arbitrary Units Measured Relative to a Known Hexamethylbenzene Sample) for Neut300 as a Function of in-Situ Temperature at Which the Data Were Recorded

temp (°C)	peak1	peak2	peak3	total area
110	100	1160	1120	1380
140	90	930	350	1370
160	630	650	150	1430
180	460	650	100	1260
200	560	440		1000

dimensions and the surface order. This is because the chemical shift will be sensitive to the surface electronic structure, and this will change. Indeed, quantum size effects may be important in these strained nanoscale systems.[27] Further, the presence of structural disorder and plane intersections at crystallite boundaries will have a strong effect on the local field. Therefore, it might be expected that peak width (sensitive to mobility and field anisotropy and so surface order) and peak position (mean surface electron density, etc.) will be sensitive to sample treatment. Thus, it should be noted that no attempt was made to reduce the sum of residuals to negligible levels. For meaningful data analysis differences between theoretical peak envelopes and experimental data were reduced while maintaining transferability of peak data. In data presented below for samples calcined at different temperatures, direct experimental evidence for four individual contributions was observed as shoulders or distinct peaks in the raw data sets. Each contribution was fitted, and only minor changes in peak position were permitted. Peak widths could be altered but were constrained to be close to the peak widths found in Figure 1 at the relevant probe temperature.

For the data collected from sample Neut300 typical curve-fitted data are shown in Figure 2. Multiple peak fitting of the data collected at 25, 50, and 80 °C is meaningless as the experimental peak width (i.e., around 3.2 ppm) due to limited mobility is much greater than the separation of each individual contribution (about 0.6 ppm minimum). At higher temperatures three peaks gave the best match to the actual spectra obtained. In this way peak positions were determined at 0.35, −0.25, and −1.15 ppm. The fwhm of these features at 180 °C were measured as 1.29, 1.53, and 0.86 ppm, respectively. The fwhm of the peaks at 0.35 and −0.25 ppm are significantly broader than might be expected. (The 0.86 ppm peak width of the −1.15 ppm feature is close to that recorded for similar data in Figure 1.) The −1.15 ppm feature is assigned to −OH species on exterior surfaces since these exterior surfaces will be essentially similar to those described in Figure 1, and the data are very similar. The other two features are assigned to −OH species at interior or pore surfaces. The increase is peak width is a reflection of either poorly ordered pore channels or of some residual template-derived species; both effects would lead to local field anisotropies. It might also be expected that some chemical shift would be observed since these pores are of nanodimensions and extremely strained.[27] Since our previous diffraction work strongly indicates that these interior surfaces are aligned so as to produce ⟨111⟩ surface planes,[10] it is suggested that the two features observed are due to adsorption at different surfaces sites. Therefore, these are very tentatively assigned to −OH species at on-top positions (0.35 ppm) and in bridging positions (−0.25 ppm). Further discussion is made below.

The curve-fitted data are summarized in Table 2 as peak areas (arbitrary units) vs probe temperature. The measured peak areas remained approximately constant to a temperature of about 160 °C and gradually decreased at 180 and 200 °C. These data were attributed to desorption of hydroxyl species (as water), causing a subsequent reduction in proton peak area. The data provided in Table 2 suggest considerable interstate conversion between bridging and on-top positions as the temperature is increased. This might be the case but is less easy to prove here. At lower temperatures errors in peak-fitting can be large as resolution of peaks is poor. Also, the experimental arrangement is not simple flow through, and in the configuration used readsorption can occur.

Very different peak shapes were obtained for the data collected from Neut400 (Figure 3), in particular the appearance of peaks with readily observed asymmetry and, at temperatures in excess of 110 °C, with the appearance of discernible shoulders. Peak widths of the data envelope were in the range 2.5−3 ppm with a mean chemical shift position of −0.4 ppm. Curve-fitting of all data consistently gave the closest match after the fitting of four peaks. A deconvoluted spectrum for the data collected at 140 °C is shown in Figure 3 (inset). The residual plot shows the close fit of the deconvoluted spectrum. Peaks derived from the curve fits had chemical shift values of 0.3, −0.3, −1.0, and −1.6 ppm with fwhm values of 0.96, 0.75, 0.76, and 0.85 ppm, respectively.

The overall peak area measured for the data collected from 25 to 200 °C is higher initially than that of Neut300 by about 50% (1860 compared to 1380, see Table 3), consistent with the exposure of more surface sites as template removal is complete and higher degrees of crystallinity are obtained at the higher calcination temperature. This supports our suggestion that broader peaks were observed for Neut300 because of these effects. The first three peaks at 0.3, −0.3, and −1.0 ppm can be readily assigned to on-top and bridging (interior surface) and on-top (exterior surface) hydroxyl species, respectively. The peak visible at −1.6 ppm has not been seen previously, but by analogy to the data from the interior surface, these data can be assigned to bridging hydroxyls at the exterior surface.

The peak area data in Table 3 also provide interesting information. Bearing in mind the likely problems in analyzing this information (see above), it is apparent that significantly more −OH is adsorbed at exterior surfaces. Peak 3 (−1.0 ppm for the on-top exterior surface species) is now a major contribution to the peak intensity. Indeed, comparing data from Neut300 and Neut400 at a probe temperature of 160 °C, the ratio of interior surfaces to exterior surfaces (assuming a coverage of one monolayer) decreases from 5.7 to 0.87. At 400 °C, the pore diameter and pore center-to-pore center distance were measured at 2.5 and 7 nm, respectively (by PXRD and BET studies).[10] Assuming a solid of hexagonal shape and infinitely long so that the pores run parallel to the length, the ratio of interior pore surface area to exterior pore surface area = pore density × circumference length of pore × length/6 × length of hexagonal face × solid length. For this material the ratio calculated is 0.87. Although this level of agreement is probably fortuitous (being an oversimplified model), it supports the original observation that Neut400 has a high degree of mesoporosity[10] and the assignment of features in this work to interior and exterior surfaces. Comment should also be made on the high peak area values recorded for Neut300. It may suggest that relatively little exterior surface is formed. This probably relates to the fact that this material is poorly ordered as a result of very low temperature calcination and probably contains a great deal of porosity other than the designed mesoporosity.

As may be expected, greater resolution of overlapping peaks at temperatures from 140 to 180 °C was observed for Neut500

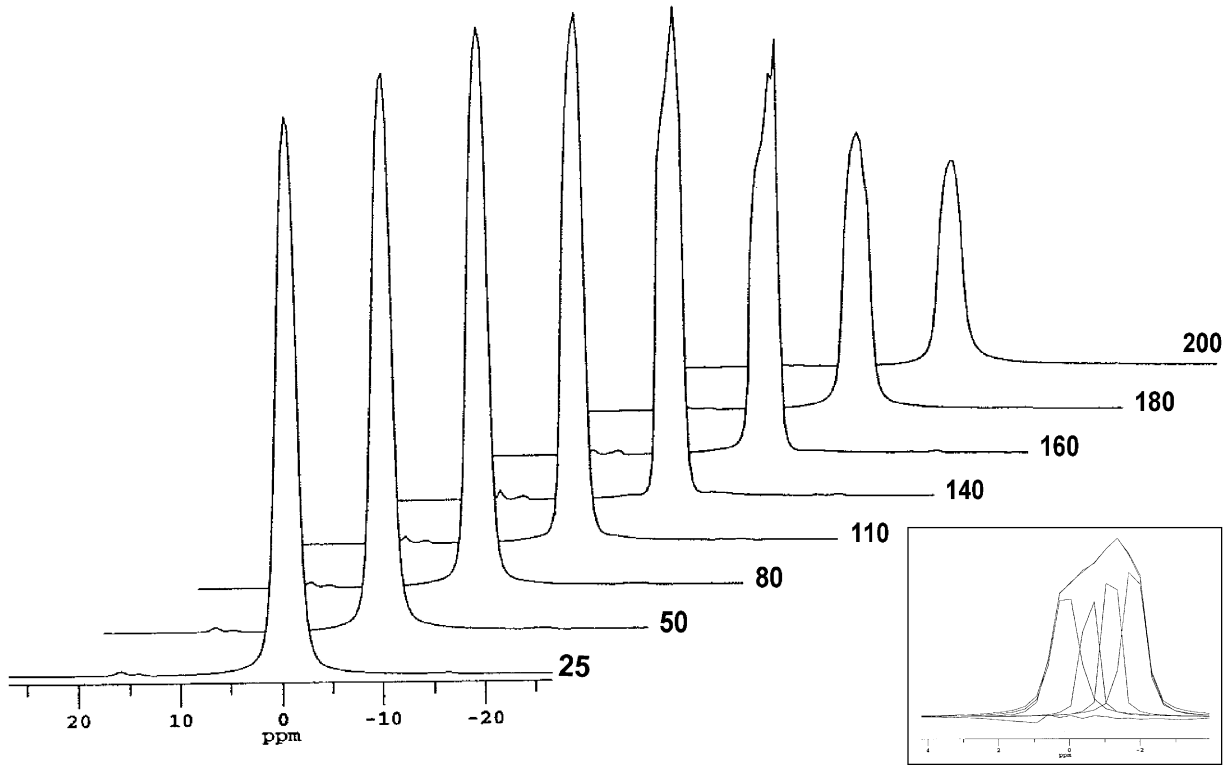

Figure 3. ^{1}H MAS NMR data collected at a series of in-situ temperatures for mesoporous ceria after calcination at 400 °C (Neut400). Deconvoluted ^{1}H MAS NMR spectrum for data collected in situ at 140 °C is shown in the inset.

TABLE 3: Peak Integrals for Neut400 Mesoporous Ceria Sample as a Function of in-Situ Temperature at Which the NMR Spectrum Was Recorded

temp (°C)	peak 1 0.3 ppm	peak 2 −0.3 ppm	peak 3 −1.0 ppm	peak 4 −1.6 ppm	total area
25	380	310	460	710	1860
50	480	340	410	580	1810
80	670	500	340	230	1740
110	330	290	390	690	1700
140	500	290	370	500	1660
160	120	500	520	300	1440
180	130	470	380	170	1150
200	90	630	70	20	810

(Figure 4). Again, the average peak position was −0.3 ppm up to 110 °C, and this decreased to −0.8 ppm for data collected at higher temperatures. Peak integral values were similar to those of Neut300 and remained relatively constant throughout the temperature range studied. At about 200 °C, there was a sharp reduction in peak areas, as in the case of other samples investigated. Deconvolution for data collected at 160 °C is shown in Figure 5. Deconvoluted peaks had chemical shifts similar to those described above at 0.5, −0.1, −0.9, and −1.5 ppm with peak widths of 0.61, 0.65, 0.58, and 0.59 ppm, respectively. While these widths are slightly less than the resolution of the NMR instrument, it should be noted that these are fitted data. The fwhm of the peak at −1.5 ppm can be experimentally measured at around 0.8 ppm. Measured peak areas as a function of probe temperature can be seen in Table 4.

It must be remembered that while curve-fitting is a reasonable indication of the number of peaks and their peak intensity, peak areas are prone to quite large errors as small changes in width can give large changes in area. Similar to the data recorded from Neut300, the total peak area remained relatively constant throughout the temperature range studied to about 140 °C when a significant reduction in peak area was observed. The ratio of interior surface hydroxyl to exterior surface hydroxyl (average of data from 25 to 140 °C) also shows a small decrease to 0.89 compared to sample Neut400. This supports our suggestions that large degrees of mesoporosity are maintained in these samples after calcination.

The ceria sample calcined at 600 °C (Neut600) displayed comparable peak splitting to Neut500, with clear peak asymmetry for data collected at 110 °C and the appearance of resolved shoulders and peaks for higher temperature spectra (Figure 5). The effective improved resolution was found to closely match deconvolution by four peaks, as with previous samples. These were observed at 0.25, −0.3, −1.1, and −1.6 ppm. The measured widths were around 0.6−0.7 ppm as for the data from Neut500. It is clear once again that desorption begins at about 160 °C. The ratio of interior surface hydroxyl to exterior surface hydroxyl (average of data from 25 to 140 °C) also shows a significant decrease (compared to data from Neut400 and Neut500) to 0.57. This continual decrease clearly indicates that mesoporosity is being lost as the calcination temperature increases. This is consistent with our previous work.[10]

It is also apparent from the total peak area data that the total amount of adsorbed hydroxyl decreases as the calcination temperature increases. Again, averaging data recorded from 25 to 140 °C, the measured values are 1790, 1734, 1546, and 1106 for samples Neut300, Neut400, Neut500, and Neut600. This decrease is in broad agreement with the measured decrease in surface area for the same samples (from 245 to 105 $m^2\ g^{-1}$). The data also suggest that a significant degree of mesoporosity is still present after calcination at 600 °C. A detailed discussion of the results is made below.

Samples of Evap600 were treated to various in-situ reduction regimes to further elucidate the nature of hydroxyl adsorption on ceria. In-situ reduction of Evap600 using a 1% H_2 in N_2

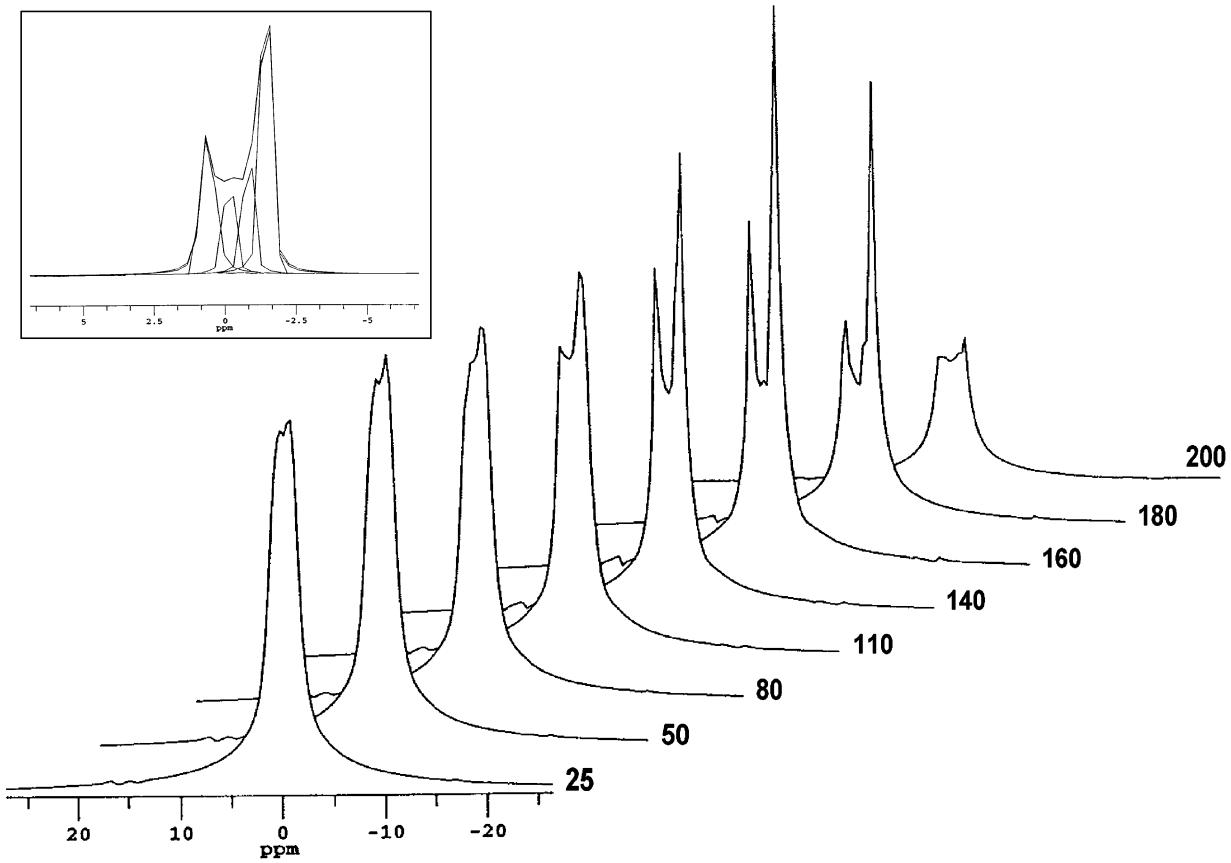

Figure 4. Plot of chemical shift vs temperature for ^{1}H MAS NMR resonance of surface-adsorbed hydroxyl species for mesoporous ceria calcined at 500 °C. Inset shows deconvoluted ^{1}H MAS NMR resonance for data collected in situ at 160 °C.

feed stream was carried out for various times, and the resulting sample was exposed to moist air for 15 min. Two resonances were observed with the peak at about 2 ppm increasing in intensity with increasing reduction time. This peak at 2 ppm is assigned to hydroxyls at reduced ceria (or defect) sites and the peak at −2 ppm to the presence of hydroxyl at the usual ceria on-top sites. Figure 7 shows data collected at 200 °C after 1 min of in-situ reduction followed by exposure to moist air for various times. Again, two peaks were evidenced and assigned to hydroxyl species at reduced ceria sites and on-top positions. However, the appearance of a shoulder to the on-top hydroxyl resonance at about −2.5 ppm and its gradual resolution into a separate peak with increasing exposure to water were also noted. The chemical shift of this hydroxyl species is near that of the hydroxyl groups on on-top positions, suggesting that this new species is in a very similar environment and therefore assigned here to hydroxyl groups on bridging positions.

Discussion

General Comments. A first general comment should be made that ^{1}H MAS NMR studies of surfaces using adsorbed hydroxyl species as probe molecules can provide interesting and valuable information particularly from powdered samples that are generally difficult to study. However, in this case, ceria may be exceptional, and the technique cannot be universally applied. Hydrogen chemical shifts are relatively small compared to instrument resolution in the MAS NMR method. The ^{1}H MAS NMR peaks observed herein are unusually narrow (if compared to materials such as SiO_2, Al_2O_3, etc.[28,29]); this has led to very difficult analysis of −OH-related features from other materials, and site adsorption data are difficult to obtain.

There are a number of reasons, of which several are structural, why the resolution of the technique is comparatively high for ceria samples. CeO_2 has a morphology dominated by exposure of the surface ⟨111⟩ plane. This vicinal plane is more thermodynamically stable at the surface than any other.[30,31] The crystallites adopt a ⟨111⟩ octahedral structure although small ⟨100⟩ plane truncations may be present.[32] In our previous work the ⟨111⟩ surface was also predominant in the case of mesoporous ceria.[10] It is also pointed out that there are no other possible polymorphs of the CeO_2 structure, and every effort was made to maintain stoichiometry to avoid reduced phases. Thus, compared to silica and alumina which are polymorphic and have an array of possible crystal planes for each structure, there are relatively few possible sites present for ceria particles. It is also important that the ceria structure has very high symmetry (*FM*3*M*) and has a relatively simple lattice. The surface has lower symmetry, but still the contribution of spinning sidebands and high field anisotropies are small.

Other factors that must be considered relate to the very high mobility of the hydroxyl species. High mobilities relate to low spin−lattice relaxation times (T_1 is around 0.001 s), and peak broadening due to saturation effects is not observed. This also allows very fast acquisition of data and signal averaging, allowing good quality data with a high signal-to-noise ratio being collected. It is also a fortuitous system as ceria is a well-known anionic conductor, and oxygen diffusion is relatively rapid compared to many other systems.[13] Note also that we have commented[13] on how the presence of long-lived electronic states can lead to T_1 times that are much longer, and in other systems where such states are formed in extended defect systems this might lead to broadening of the signals. Indeed in this system, if chemical reduction (i.e., hydrogen gas is used in the probe)

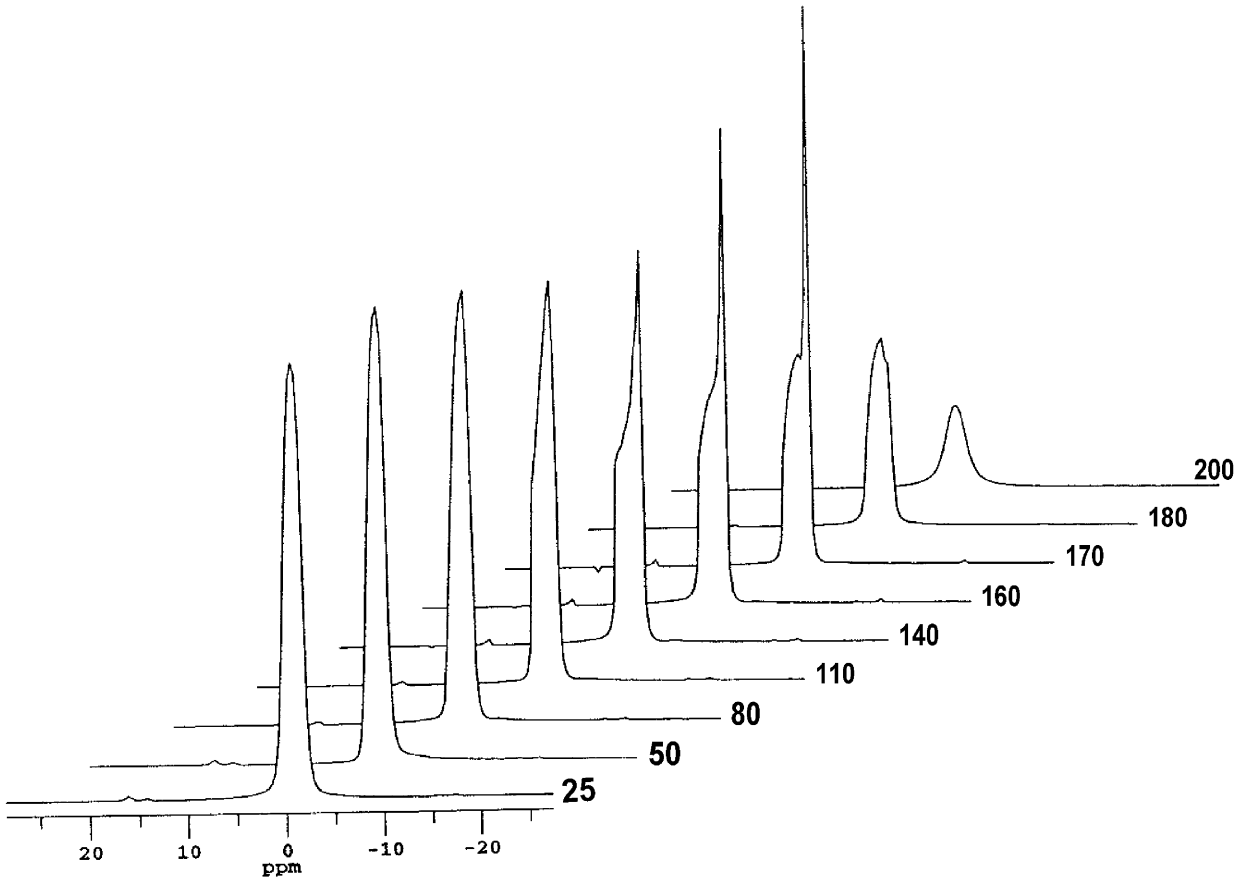

Figure 5. [1]H MAS NMR data recorded for Neut600 as a function of in-situ temperature (as shown, °C).

TABLE 4: Peak Integrals for Neut500 Mesoporous Ceria Sample as a Function of in-Situ Probe Temperature at Which the NMR Spectrum Was Recorded

temp (°C)	peak 1 0.25 ppm	peak 2 −0.3 ppm	peak 3 −1.2 ppm	peak 4 −1.6 ppm	total area
25	150	340	370	250	1110
50	170	330	390	210	1100
80	190	320	380	220	1110
110	170	90	250	600	1110
140	160	90	440	410	1100
160	220	120	200	500	1040
180	140	280	240	340	1000
200	50	170	310	50	580

is carried out, a broad signal appears at around 2−4 ppm with resonance widths up to 4 times greater than for the species observed here. Illustrative data are given in Figure 6, which shows the effect of raising the probe temperature during exposure to a 1% H_2−99% N_2 gas stream. As the temperature is raised, the amount of reduction is reflected by the increase in intensity of the feature with the high chemical shift. The electronic band structure which has effects on the local fluctuating fields must also be considered. This contribution to peak broadening is minimal as ceria has a closed-shell electronic configuration (vacant 4s, 4f and full 3d levels) with only deep-lying populated electron orbitals. It is hard to think of another system where all these conditions are met. As a result, ceria may be a unique system which provides an ideal opportunity for hydroxyl probe molecule MAS NMR studies as the observed [1]H features have peak widths close to what might be recorded for a liquid sample on this apparatus.

Comments on Peak Assignment. Infrared spectroscopy suggests that on defect-free crystalline ceria surfaces there are

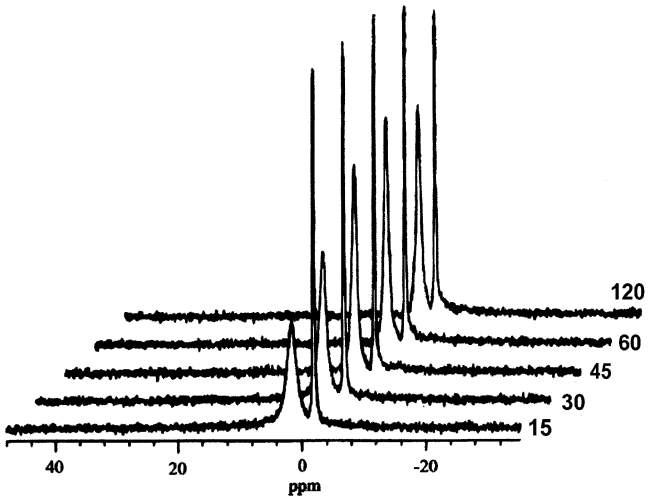

Figure 6. [1]H MAS NMR resonances from a sample of Evap600 after reduction at 200 °C in a hydrogen−nitrogen mix for various times (in minutes) followed by in-situ exposure to water for 15 min.

two probable positions that −OH groups may occupy; these can be described as on-top and bridging.[33] The ceria ⟨111⟩ surface is complex. It is puckered with a symmetrical distorted hexagonal arrangement of alternating in-plane, out-of-plane cations and anions. All on-top positions are equivalent while two chemically distinct bridge sites exist. As the MAS NMR proton resolution is high, it is possible that these sites can be resolved. The data presented here suggest that only one of the bridge sites is occupied. For the nonporous sample where essentially one principal surface hydroxyl species is observed, it is logical to assign the feature to on-top hydroxyl species as

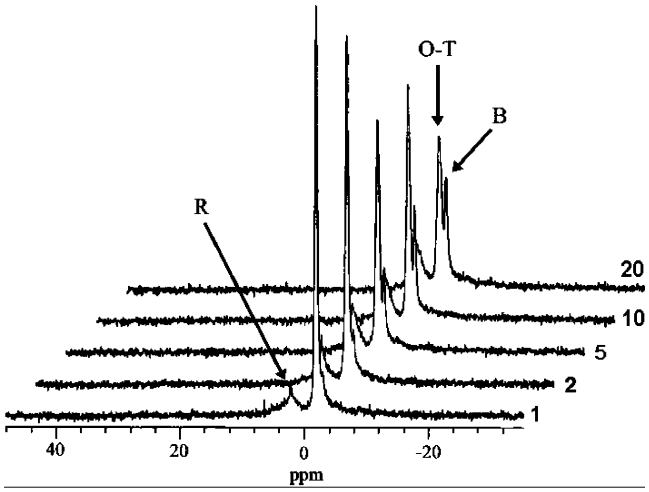

Figure 7. ^{1}H MAS NMR resonances from a sample of Evap600 after reduction at 200 °C in a hydrogen−nitrogen mix for 1 min followed by exposure to water in the usual manner for varying times (shown in minutes). The peak, R, at about 2 ppm is assigned to reduced ceria. The resonance marked O-T is the usual on-top hydroxyl feature, and the resonance marked B is assigned to bridging sites.

this is most likely adsorption position.[33] In this way features at −1.0 to −1.2 ppm are assigned to on-top hydroxyl species at exterior surfaces.

In the case of porous compounds there are two different surface regions, namely exterior (at the surfaces defining the particle morphology) and interior (those that act as pore walls). Our previous work shows that these interior surfaces also have a ⟨111⟩ surface orientation.[10] However, because of finite size effects and strain, the electronic structure of the crystal lattice will be different in this environment than that of the external crystal surface.[27] It should be pointed out that nanoporous ceria has quite different electronic and ionic conductivity and chemical properties compared to those of bulk ceria.[34−36] In this way, it might be expected that new NMR resonances will be observed arising from hydroxyl groups confined within the pores of a mesoporous material. Again, these will be expected in the same on-top or bridging positions as in the case of external surfaces. It is therefore expected that there are four different environments that may give rise to individual signals, and it would appear that these are observed in the experiments reported here. The additional peaks seen for the mesoporous samples may also partly arise from the existence of new sites, for example, such as those present on ⟨100⟩ planes (see above). However, the experimental evidence points to a great majority of ⟨111⟩ surface planes,[10] and the ⟨111⟩ surface is so much higher in stability[30,31,37] that the importance of additional planes can be largely ignored. This is especially true as the features do have similar intensities.

As discussed previously, these interior surfaces will be highly strained because of pore wall curvature. They might, in very simple terms, be considered to be rougher and more defective than external surfaces which are much more extended. Thus, it might be expected that electron density at the internal surface is lower than for external surfaces. Lower electron density would favor deshielding of the protons, and thus a downfield (i.e., to more positive ppm) shift is expected. In this way peaks around 0.5−0.2 ppm and −0.2 to −0.5 ppm are assigned to hydroxyls at interior and exterior surfaces, respectively. This assignment is consistent with the facts that these features are very minor in the densified (Evap600) sample, the trend in mesoporosity expected with increasing calcination temperature and simple calculations based on the known pore structure.[10] The assignment is also consistent with the T_1 relaxation times measured. Surface migration on external areas is less restricted than on internal pore surfaces. Since spin−lattice relaxation is related to mobility, it might be expected that there are shorter T_1 times for the more mobile exterior species, and this is indeed observed (see Table 1).

In each series of NMR data there is a loss of −OH-derived ^{1}H intensity with increasing probe temperature. This observation is consistent with the gradual desorption of surface hydroxyl species from ceria at temperatures in excess of 160 °C. This is consistent with literature values for the onset of water desorption.[38] Unfortunately, it is not possible to clearly define events such as interstate conversion in these results. The sample is highly constrained (in terms of gas flow and is tightly packed during spinning), and the energy due to very high spinning rates ensures that effects such as readsorption and mechanical desorption complicate the data and make interpretation difficult.

Resolution of the spectra into four peaks has prompted us to assign features around −0.3 and −1.5 ppm to adsorption on bridging sites at interior and exterior surfaces, respectively. We have argued that the morphology of ceria particles ensures the predominant surface is of ⟨111⟩ orientation, and contributions from other crystal planes are unlikely. The shifts from the on-top hydroxyl-derived resonances are small (about −0.5 ppm) and are unlikely to be due to non −OH species. It was noted the very fast spinning speeds ensure no water physisorption is possible, and at the end of experiments no carbon species (which might produce a shift) could be detected by ^{13}C cross-polarization MAS NMR. In this way the data represent two doublets for interior and exterior surfaces, and each doublet represents a downfield (on-top hydroxyl species) and an upfield (bridging hydroxyl species) component. This assignment is consistent with the shift observed since the bridging species might be expected to be more shielded than on-top species.

One question that needs to be addressed is why bridging type species are not observed in the data from the densified Evap600 sample shown in Figure 1. The answer seems to be related to the presence of defects which appear to promote the presence of bridging species. In Figure 7 the Evap600 sample was cleaned by extended in-situ heating at 200 °C in air. The sample was reduced by subsequent exposure (200 °C) to the hydrogen−nitrogen reducing gas (1% H_2−9% N_2) mixture for 1 min before exposure to water. It can be seen immediately that, as well as the expected on-top hydroxyl adsorption at −1.2 ppm, a feature is initially seen as a shoulder at −1.6 ppm, and as exposure continues this shoulder becomes a well-resolved peak. Noticeable also is the increasing width of the resonance attributable to on-top adsorption as exposure increases—it seems likely that the presence of bridging −OH species limits the mobility of the on-top hydroxyls. It is concluded that for the mesoporous samples formation of bridging species is promoted by the highly strained nature of the pore surfaces.

Properties of Mesoporous Ceria. In previous work it was suggested that mesoporous ceria was quite an unusual material consisting of a hexagonal arrangement of pores with ordered crystalline walls.[10] The data presented herein are consistent with this description as the mesoporous materials produce very sharp ^{1}H MAS NMR resonances consistent with the presence of highly ordered interior and external surfaces of low field anisotropies. The narrow width of the NMR peaks is due to very high mobility of the hydroxyl species, which again suggests that the internal pore surfaces are highly ordered as plane dislocations etc. would contribute significant additional barriers to surface

diffusion.[39] Since the features observed from internal and external surfaces have very similar peak widths and chemical shifts, it is clear these surfaces are very closely related, and this again is an indication that similar surface geometries are present.

However, the internal surface ⟨111⟩ planes are quite chemically distinct from exterior surfaces. As shown by the measurement of the ^{1}H chemical shift of the hydroxyl species, these features are shifted to higher ppm values than on the exterior surfaces. It is argued that this is due to lower surface electron densities consistent with the strained geometry of the internal surfaces. This observation suggests that the chemical properties of mesoporous ceria might be quite different when compared to that of bulk ceria. This might indicate that in catalysis there may be additional benefits (or disadvantages) to nanostructured ceria besides simply exhibiting proportionally higher surface areas than nonmesoporous samples. The ability to change electronic and chemical properties of materials through mesoporous synthesis routes should provide further impetus to develop preparation routes to other mesoporous materials.

Finally, MAS NMR has proved a versatile method of exploring the surface chemistry of these nanostructured materials. As more and more work in the area of nanoscience is being carried out, MAS NMR will provide a useful additional method of studying the surfaces of these important materials. Surface science has constantly striven toward developing techniques for the study of real surfaces in real conditions. Studying powdered materials of very small particle sizes has been difficult because of limitations in diffraction and some spectroscopy methods. MAS NMR is particularly useful because of its sensitivity to local rather than very long-range environments. In the course of this work attempts were made to study the surfaces by infrared spectroscopy, but data showing only very broad features were observed, highlighting the usefulness of employing MAS NMR as a practical means of studying these surfaces. However, as discussed above, the general application of MAS NMR techniques to other systems might be more limited although such investigations should be made to juxtapose the data presented herein.

Conclusion

The complexity of the ceria system and the observation of enhanced ionic, electronic, and catalytic properties by manipulating the structure on a nanometer scale are continuing to motivate research into nanocrystalline ceria. ^{1}H MAS NMR spectroscopy of adsorbed hydroxyl species is shown to be a useful investigative technique for probing the nature of solid oxide surfaces. It is sensitive to low concentrations of adsorbed hydroxyl (0.1% of saturation surface coverage) and can be used to detect adsorption at defect surface sites. Here is the first reported MAS NMR study of mesoporous ceria. Sharp proton resonances were obtained for all samples, and at elevated in-situ temperatures clear peak asymmetry and splitting were evidenced. This suggests that there is more than one proton environment and consequently different hydroxyl adsorption sites. Four proton resonances were typically observed and assigned to −OH groups on cerium atoms in bridging and on-top positions on both internal and external surfaces. Such internal surfaces are present due to the highly porous nature of these materials. Chemical shift data suggest that electron donation from ceria to the adsorbed species is significant and results in increased shielding and a consequent shift to higher field. This effect was greater for hydroxyl groups adsorbed on external surfaces than for species adsorbed on pore walls and shows that these surfaces have differing electronic properties consistent with the strain at these surfaces. It is also shown that the internal pore surfaces and external surfaces have essentially the same surface structural arrangements, exhibiting very narrow resonances and surface mobilities for the adsorbed species.

Acknowledgment. The authors very kindly thank Prof. J. Cunningham for all the help and encouragement he gave through this work. The authors thank Dr. Paul Jonsen of Bruker for many helpful discussions, suggestions, and reading of the data. D.M.L. acknowledges financial assistance from Enterprise Ireland under Project BR/1997/198. We also thank the HEA Large Equipment Fund for provision of the equipment used.

References and Notes

(1) Tranquada, J. M.; Heald, S. M.; Moodenbaugh, A. R.; Liang, G.; Croft, M. *Nature (London)* **1989**, *337*, 720.
(2) Kim, G. *Ind. Eng. Chem. Prod. Res. Dev.* **1982**, *21*, 267.
(3) Liu, B.; Wagberg, T.; Olsson, E.; Yang, R.; Li, H.; Zhang, S.; Yang, H.; Zou, G.; Sundqvist, B. *Chem. Phys. Lett.* **2002**, *320*, 365.
(4) Putna, E. S.; Stubenrauch, J.; Vohs, J. M.; Gorte, R. J. *Langmuir* **1995**, *11*, 4832.
(5) Schroder, A.; Aeppli, G.; Coldea, R.; Adams, M.; Stockert, O.; Lohneysen, H.v.; Bucher, E.; Ramazashvili, R.; Coleman, P. *Nature (London)* **2000**, *407*, 351.
(6) Skorodumova, N. V.; Simak, S. I.; Lundqvist, B. I.; Abrikosov, I. A.; Johansson, B. *Phys. Rev. Lett.* **2002**, *89*, 166601.
(7) Mamontov, E.; Egami, T.; Brezny, R.; Koranne, M.; Tyagi, S. *J. Phys. Chem. B* **2000**, *104*, 11110.
(8) Patsalas, P.; Logothetides, S.; Metaxa, C. *Appl. Phys. Lett.* **2002**, *81*, 466.
(9) Wang, J. A.; Dominguez, J. M.; Montoya, A.; Castillo, S.; Navarrete, J.; Moran-Pineda, M.; Reyes-Gasca, J.; Bokhimi, X. *Chem. Mater.* **2002**, *14*, 4676.
(10) Lyons, D. M.; Ryan, K. M.; Morris, M. A. *J. Mater. Chem.* **2002**, *12*, 1207.
(11) Cordatos, H.; Bunluesin, T.; Stubenrauch, J.; Vohs, J. M.; Gorte, R. J. *J. Phys. Chem.* **1996**, *100*, 785.
(12) Martinez-Arias, A.; Soria, J.; Conesa, J. C. *J. Catal.* **1997**, *168*, 364.
(13) O'Neill, W. M.; Morris, M. A. *Chem. Phys. Lett.* **1999**, *305*, 389.
(14) Castellani, F.; Van Rossum, B.; Diehl, A.; Schubert, M.; Rehbein, K.; Oschkinat, H. *Nature (London)* **2002**, *420*, 98.
(15) Pichler, M.; Knicker, H.; Kogel-Knabner, I. *J. Ind. Microbiol. Biotechnol.* **2001**, *26*, 83.
(16) Jacobsen, C. J. H.; Madsen, C.; Janssens, T. V. W.; Jakobsen, H. J.; Skibsted, J. *Microporous Mesoporous Mater.* **2000**, *39*, 393.
(17) Karger, J.; Pfeifer, H.; Wutscherk, T.; Ernst, S.; Weitkamp, J.; Fraissard, J. *J. Phys. Chem.* **1992**, *96*, 5059. Forste, C.; Karger, J.; Pfeifer, H. *J. Am. Chem. Soc.* **1990**, *112*, 7.
(18) Heink, W.; Karger, J.; Pfeifer, H.; Stallmach, F. *J. Am. Chem. Soc.* **1990**, *112*, 2175.
(19) Terskikh V. V.; Moudrakovski, I. L.; Breeze, S. R.; Lang, S.; Ratcliffe, C. I.; Ripmeester, J. A.; Sayari, A. *Langmuir* **2002**, *18*, 5653.
(20) Batamack, P.; Doremieux-Morin, C.; Fraissard, J.; Freude, D. *J. Phys. Chem.* **1991**, *95*, 3790.
(21) Schmidt, R.; Hansen, E. W.; Stocker, M.; Akporiaye, D. E.; Ellestad, O. H. *J. Am. Chem. Soc.* **1995**, *117*, 4049.
(22) Hansen, E. W.; Schmidt, R.; Stocker, M.; Akporiaye, D. *J. Phys. Chem.* **1995**, *99*, 4148.
(23) Bulanin, K. M.; Lavalley, J. C.; Lamotte, J.; Mariey, L.; Tsyganenko, N. M.; Tsyganenko, A. A. *J. Phys. Chem. B* **1998**, *102*, 6809.
(24) Madier, Y.; Descorme, C.; Le Govic, A. M.; Duprez, D. *J. Phys. Chem. B* **1999**, *103*, 10999.
(25) Mills, R. *J. Phys. Chem.* **1973**, *77*, 685.
(26) Terribile, D.; Trovarelli, A.; de Leitenburg, C.; Dolcetti, G. *Chem. Mater.* **1997**, *9*, 2676.
(27) Lyons, D. M.; Ryan, K. M.; Morris, M. A.; Holmes, J. D. *Nano Lett.* **2002**, *2*, 811.
(28) Kolodziejski, W.; Corma, A.; Navarro, M. T.; Pariente, J. P. *Solid State Nucl. Magn. Reson.* **1993**, *2*, 253.
(29) Gao, Q.; Chen, J.; Ruren, X.; Yue, Y. *Chem. Mater.* **1997**, *9*, 457.
(30) Vyas, S.; Grimes, R. W.; Gay, D. H.; Rohl, A. L. *J. Chem. Soc., Faraday Trans.* **1998**, *94*, 427.
(31) Conesa, J. *Surf. Sci.* **1995**, *339*, 337.
(32) Lee, W.-H.; Shen, P. *J. Cryst. Growth* **1999**, *205*, 169.

(33) Badri, A.; Binet, C.; Lavalley, J. C. *J. Chem. Soc., Faraday Trans.* **1997**, *93*, 1159.
(34) Tschope, A.; Birringer, R. *J. Electroceram.* **2001**, *7*, 169.
(35) Chiang, Y.-M.; Lavik, E. B.; Kosacki, I.; Tuller, H. L.; Ying, J. Y. *J. Electroceram.* **1997**, *1*, 7.
(36) Tschope, A.; Birringer, R. *Nanostruct. Mater.* **1997**, *9*, 591.
(37) Baudin, M.; Wojcik, M.; Hermansson, K. *Surf. Sci.* **2000**, *468*, 51.
(38) Cunningham, J.; Cullinane, D.; Sanz, J.; Rojo, J. M.; Soria, X. A.; Fierro, J. L. G. *J. Chem. Soc., Faraday Trans.* **1992**, *88*, 3233.
(39) Morris, M. A.; Bowker, M.; King, D. A. In *Comprehensive Chemical Kinetics*; Tipper, C. F. H., Bamford, C. H., Compton, R. G., Eds.; Elsevier: Amsterdam, 1985; Vol. 25.